

Validation of the land-surface temperature products retrieved from Terra Moderate Resolution Imaging Spectroradiometer data

Zhengming Wan^{a,*}, Yulin Zhang^a, Qincheng Zhang^a, Zhao-liang Li^{a,b}

^aICESSE, University of California, Santa Barbara, CA 93106-3060, USA

^bGRTR/LSIT/ENSPS, Parc d'Innovation, 5 Bd. Sebastien Brant, 67400 Illkirch-Graffenstaden, France

Received 13 December 2001; received in revised form 6 March 2002; accepted 1 April 2002

Abstract

This paper presents the status of land-surface temperature (LST) standard products retrieved from Earth Observing System (EOS) Moderate Resolution Imaging Spectroradiometer (MODIS) data. Based on estimates of the channel-dependence error and noise equivalent temperature difference (NEDT) and the calibration accuracy of MODIS thermal–infrared data, the impact of instrument performance on the accuracy of LST is discussed. A double-screen scheme based on the difference between the 5-km LST retrieved by the day/night LST algorithm and the aggregated 1-km LST retrieved by the generalized split-window algorithm, and the difference between daytime and nighttime LSTs, is proposed to remove the LSTs contaminated with cloud effects. The accuracy of daily MODIS LST product at 1-km resolution, which was produced by the generalized split-window algorithm, was validated in 11 clear-sky cases with in situ measurement data collected in field campaigns in 2000 and 2001. The MODIS LST accuracy is better than 1 K in the range from 263 to 300 K over Lake Titicaca in Bolivia, Mono Lake, Bridgeport grassland, and a rice field in Chico, CA, and Walker Lake, Nevada (NV), in the atmospheric column water vapor range from 0.4 to 3.0 cm. It is difficult to validate the daytime LST product over land sites rather than lakes with ground-based measurements alone because of the high spatial variations in the in situ LST measurement data, which was verified by the daytime data of the MODIS Airborne Simulator (MAS) over a grassland in Bridgeport, CA, on October 6, 2000. In six cases over a silt playa in Railroad Valley, NV, the 1-km MODIS LSTs are a few Kelvin degrees lower than the in situ measured LSTs because the surface emissivities inferred from land cover types in the split-window LST method are often overestimated in semi-arid and arid regions. After a correction with the difference between the 5-km LST retrieved by the day/night LST method and the LST aggregated from 1-km LSTs retrieved by the split-window method, the MODIS LSTs agree with in situ measured LSTs within ± 1 K in the range 263–322 K for the six cases in Railroad Valley and one case of snowcover in Bridgeport, CA, leading a recommendation for use of the 5-km LST product retrieved by the day/night LST method in bare and sparse vegetated areas.

© 2002 Elsevier Science Inc. All rights reserved.

1. Introduction

Land-surface temperature (LST) is one of the key parameters in the physics of land-surface processes on regional and global scales, combining the results of all surface–atmosphere interactions and energy fluxes between the atmosphere and the ground (Mannstein, 1987; Sellers, Hall, Asrar, Strebel, & Murphy, 1988). One of the most important potential applications of the LST retrieved from satellite data is to validate and improve the global meteorological model prediction after appropriate aggregation and param-

eterization (Price, 1982; Diak & Whipple, 1993). Besides its necessity in the LST retrieval, the surface emissivity can be used to discriminate senescent vegetation (French, Schmugge, & Kustas, 2000a). The remotely sensed LST has been used in land cover and land-cover change analysis (Ehrlich & Lambin, 1996; Lambin & Ehrlich, 1997) and in the production of the Moderate Resolution Imaging Spectroradiometer (MODIS) land cover product, in estimation and parameterization of surface fluxes (Brutsaert, Hsu, & Schmuuge, 1993; French, Schmugge, & Kustas, 2000b), and in estimating the diurnal cycle (Jin & Dickinson, 1999). LST can be also used to monitor drought and estimate surface soil moisture (Feldhake, Glenn, & Peterson, 1996; McVicar & Jupp, 1998), to evaluate water requirements of wheat (Jackson, Reginato, & Idso, 1977) and to determine frosts in orange groves (Caselles & Sobrino, 1989).

* Corresponding author. Tel.: +1-805-893-4541; fax: +1-805-893-2578.
E-mail address: wan@icess.ucsb.edu (Z. Wan).

Remote sensing of sea-surface temperature (SST) has been a primary function of satellite infrared radiometers since their inception. And starting from 1982, the SST derived from NOAA Advanced Very High Resolution Radiometer (AVHRR) data has been included in the high-resolution global SST climatology data set for global change studies (Brown, Evans, & Cornillon, 1991; Smith & Reynolds, 1998). In comparison, there is no standard global LST data product derived from satellite remote sensing data even though the use of thermal–infrared (TIR) measurements for analysis of land biophysical conditions has been under investigation for more than three decades (Fuchs & Tanner, 1966) and the AVHRR data have been used to produce LST data in the development of LST algorithms for two decades. It is well known that simple extension of the SST methods to LST for AVHRR data would lead to unacceptable errors (Price, 1984; Becker, 1987) because of the difficulty in cloud detection with AVHRR data over land (especially for thin cirrus) and the intrinsic difficulties in the LST retrieval (Wan & Dozier, 1989).

The MODIS (Salomonson, Barnes, Maymon, Montgomery, & Ostrow, 1989) onboard the first Earth Observing System (EOS) platform (called Terra), which was successfully launched on December 18, 1999, provides a new opportunity for global studies of atmosphere, land, and ocean processes (King, Kaufman, Menzel, & Tanré, 1992; Justice et al., 1998; Esaias et al., 1998), and for satellite measurements of global LST. The strengths of MODIS include its global coverage, high radiometric resolution and dynamic ranges suitable for atmosphere, land, or ocean studies, and accurate calibration in multiple TIR bands designed for retrievals of SST, LST and atmospheric properties. Specifically, band 26 will be used to detect cirrus clouds (Gao & Kaufman, 1995), band 21 for fire detection (Kaufman et al., 1998), all other TIR channels will be used to retrieve atmospheric temperature and water vapor profiles (Smith, Woolf, & Schriener, 1985), and TIR bands 20, 22, 23, 29, 31–33 will correct for atmospheric effects and retrieve surface emissivity and temperature (Wan & Li, 1997). This paper will present the heritage of LST algorithms, the MODIS LST algorithms, a summary of performance of MODIS TIR bands and its impact on the accuracy of retrieved LST, a brief description of the MODIS LST products, and the LST validation results in the following sections.

2. Heritage for LST remote sensing

A variety of LST methods have been published in the open literature. Here we provide some examples rather than a complete review. LST can be retrieved from a single infrared channel through an accurate radiative transfer model if surface emissivity is known and temperature/water vapor profile is given by either satellite soundings or conventional radiosonde data (Price, 1983; Susskind, Rosenfield, Reuter, & Chahine, 1984; Chedin, Scott, Wahiche, & Moulinier,

1985; Ottlé & Vidal-Madjar, 1992). Split-window LST methods require known surface emissivities to make corrections for the atmospheric and surface emissivity effects based on the differential atmospheric absorption in the 10–13 μm split window without knowledge of the atmospheric temperature/water vapor profile although column water vapor is used in some split-window LST algorithms to improve the accuracy of LST retrieval (Price, 1984; Becker, 1987; Wan & Dozier, 1989; Becker & Li, 1990; Sobrino, Coll, & Caselles, 1991; Vidal, 1991; Kerr, Lagouarde, & Imbernon, 1992; Ottlé & Stoll, 1993; Prata, 1994; Wan & Dozier, 1996). Because the accuracy of LST retrieved by single channel methods and split-window methods depends on the accuracy of surface emissivity, these methods do not work well in semi-arid and arid regions, where surface emissivity may vary significantly with location and time.

Methods which extract relative emissivities from multi-spectral TIR data include reference channel method (Kahle, Madura, & Soha, 1980), emissivity normalization method (Gillespie, 1985; Realmuto, 1990), temperature-independent spectral indices (TISI) method (Becker & Li, 1990), spectral ratio method (Watson, 1992), and alpha residuals method (Kealy & Gabell, 1990). Li, Becker, Stoll, and Wan (1999) compares these methods with simulated TIMS (Thermal Infrared Multispectral Scanner) data, and shows that all these methods are sensitive to the uncertainties of atmosphere and an error of 20% in water vapor in mid-latitude summer atmosphere may lead to an error up to 0.03 in the relative emissivity in channel 1 of TIMS (at 8.379 μm), and the alpha method is even worse.

The TISI-based day/night method (Becker & Li, 1990) uses a pair of day/night co-registered AVHRR TIR data to estimate the bidirectional reflectance in channel 3, and then estimates emissivity in this channel based on the Lambertian assumption of surface reflectance (Becker & Li, 1990) or a priori knowledge of bidirectional reflectance distribution function (BRDF) (Li & Becker, 1993), emissivities in channels 4 and 5 with TISI, and finally estimates LST with the single channel method or the split-window method. If there are enough pairs of day/night co-registered AVHRR TIR data in a relative short period of time ranging from a few weeks to a few months depending on location and season in which surface BRDF does not change substantially and atmospheric temperature/water vapor profiles are available, directional emissivities at a series of view angles can be estimated using the integration of BRDF values in channel 3 estimated from AVHRR data (Nerry, Petitcolin, & Stoll, 1998).

The temperature and emissivity separation algorithm for Advanced Spaceborne Thermal Emission and Reflection Radiometer (ASTER) (Gillespie et al., 1998) inherits features of the normalization method and spectral ratio method, and uses an empirical relationship of maximum–minimum emissivity difference (MMD) to refine estimates of surface emissivities and temperature.

In the above LST methods, only split-window methods do not require accurate atmospheric temperature/water vapor profile. Errors in emissivity and LST retrieved from all other methods depend on uncertainties in the input atmospheric profile. It is well known that there are large spatial and temporal variations in atmospheric water vapor. Padilla, Leyva, and Mosino (1993) made psychrometric measurements for study of atmospheric humidity behavior at two places in Mexico, one in the Chaoultepec Heights, in the western zone of Mexico City at 2300 m above sea level, and another in Rancho Viejo, a mountainous wooded area at 2700 m above sea level. The distance between these places is approximately 68 km. They found that the mixing ratio mean values for clear-sky days in the 1989 rainy season vary 30% during 9:00–12:00 local time, and 40% in 12:00–15:00. Bruegge et al. (1992) reported that water vapor column abundances retrieved from the Airborne Visible Infrared Imaging Spectrometer (AVIRIS) data during the First ISLSCP Field Experiment (FIFE) over the Konza Prairie, Kansas, on August 31, 1990, indicated that the spatial variability over scales associated with surface topography and the underlying vegetation may be greater than 10%.

Because of the close coupling between land surface and atmosphere, small changes in surface emissivities cause measurable changes in infrared radiances so that uncertainties in surface emissivities may result in large errors in the atmospheric temperature/water vapor retrieval (Plokhenko & Menzel, 2000). Therefore, we have to consider the potentially large uncertainties in the atmospheric temperature/water vapor profiles retrieved from satellite TIR data when we use the atmospheric profiles in the estimates of land-surface emissivity and temperature, especially in areas where surface emissivities are in low values and highly variable.

3. MODIS LST algorithms

3.1. The generalized split-window LST algorithm

The LST of clear-sky pixels in MODIS scenes is retrieved with the split-window algorithm in a general form (Wan & Dozier, 1996)

$$T_s = C + \left(A_1 + A_2 \frac{1 - \varepsilon}{\varepsilon} + A_3 \frac{\Delta\varepsilon}{\varepsilon^2} \right) \frac{T_{31} + T_{32}}{2} + \left(B_1 + B_2 \frac{1 - \varepsilon}{\varepsilon} + B_3 \frac{\Delta\varepsilon}{\varepsilon^2} \right) \frac{T_{31} - T_{32}}{2}, \quad (1)$$

where $\varepsilon = 0.5(\varepsilon_{31} + \varepsilon_{32})$, and $\Delta\varepsilon = \varepsilon_{31} - \varepsilon_{32}$ are the mean and the difference of surface emissivities in MODIS bands 31 and 32. T_{31} and T_{32} are the brightness temperatures in these two split-window bands. The coefficients C , A_i and B_i , $i = 1, 2, 3$, are given by interpolation on a set of multi-dimensional look-up tables (LUT). The LUTs were obtained by linear regres-

sion of the MODIS simulation data from radiative transfer calculations over wide ranges of surface and atmospheric conditions. Improvements for the generalized split-window LST algorithm incorporated in the establishment of the LUTs include: (1) view-angle dependence, (2) column water vapor dependence, and (3) dependence on the atmospheric lower boundary temperature. The view-angle dependence is kept in one dimension of LUTs for a set of viewing angles covering the whole MODIS swath so that LST can be retrieved at higher accuracies for pixels at both small and large viewing zenith angles, and at best accuracies for pixels at nadir and small view angles. The column water vapor dependence is kept in another dimension of LUTs for a set of overlapping intervals of column water vapor so that the information of water vapor provided in the MODIS atmospheric product is used as the most likely range of the water vapor rather than its exact value because the uncertainties in the atmospheric water vapor may be large. Similarly, the information of the atmospheric lower boundary temperature (T_{air}) provided in the MODIS atmospheric product is also used to improve the LST retrieval accuracy. The LST accuracy can be improved further by iterations with the information of difference between surface temperature T_s and T_{air} .

The band emissivities, also called classification-based emissivities (Snyder, Wan, Zhang, & Feng, 1998), are estimated from land cover types in each MODIS pixel through TIR BRDF and emissivity modeling (Snyder & Wan, 1998). A simple linear correction is made to the band emissivities to account for the viewing angle effect in the emissivities when the viewing angle is larger than 45° for some land cover types. In the at-launch MODIS LST processing, the University of Maryland IGBP-type land-cover based on AVHRR data (Townshend et al., 1994) is used to provide global land cover information at 1-km grids. Since June 2001, the MODIS land-cover product (Murchoney et al., 1999) is used in the MODIS LST processing. Note that errors and uncertainties in the classification-based emissivities may be large in semi-arid and arid regions because of the large temporal and spatial variations in surface emissivities and lack of knowledge on the emissivity variation with viewing angle.

3.2. The MODIS day/night LST algorithm

A physics-based day/night algorithm (Wan & Li, 1997) was developed to retrieve surface spectral emissivity and temperature at 5-km resolution from a pair of daytime and nighttime MODIS data in seven TIR bands, i.e., bands 20, 22, 23, 29, and 31–33. The inputs to this algorithm include the MODIS calibrated radiance product (MOD021KM), geolocation product (MOD03), atmospheric temperature and water vapor profile product (MOD07), and cloudmask product (MOD35). To our knowledge, this day/night algorithm is the first operational LST algorithm capable of adjusting the uncertainties in atmospheric temperature and water vapor profiles for a better retrieval of the surface

emissivity and temperature without a complicated complete retrieval of surface variables and atmospheric profiles simultaneously (Ma et al., 2000, Ma, Wan, Moeller, Menzel, Gumley, & Zhang, 2002). Because we use a pair of daytime and nighttime MODIS data in seven bands, we have 14 observations. In the day/night algorithm, there may be maximum of 14 unknown variables. The minimal set of the surface variables includes seven band emissivities, and daytime and nighttime surface temperatures. There are only five unknowns left for atmospheric variables. Because of the close coupling between land surface and atmosphere, uncertainties in surface emissivities may result in large errors in the atmospheric temperature/water vapor retrieval (Ploshenko & Menzel, 2000). These errors could exist in the shape of the retrieved temperature/humidity profile, and in the values of atmospheric temperature at the surface level (T_a) and column water vapor (cwv). Atmospheric radiative transfer simulations show that the MODIS radiances in the above seven TIR bands are relatively less sensitive to changes in the shapes of temperature and water vapor profiles. Therefore, we set four atmospheric variables (T_a and cwv, for daytime and nighttime, respectively). Then there is only one unknown left for the anisotropic factor of the solar beam BRDF at the surface. This anisotropic factor is defined by the ratio of the surface-reflected solar beam at the view direction of the MODIS sensor to the radiance that would have resulted if the surface reflected isotropically (such a surface is called Lambertian surface),

$$\alpha = \frac{\pi f_r(\mu; \mu_0, \phi_0)}{r}, \quad (2)$$

where r is reflectance of the assumed Lambertian surface. Bidirectional reflectance measurements of sands and soils (Snyder, Wan, Zhang, & Feng, 1997) show that although there are quite strong spectral variations in surface reflectance for most terrestrial materials in the 3.5–4.2 μm wavelength range, their BRDF anisotropic factor in this wavelength range has very small variations on the order of 2%. Therefore, we can use a single anisotropic factor for bands 20, 22, and 23. Besides, we assume the following: (1) The surface emissivity changes with vegetation coverage and surface moisture content. However, it does not significantly change in several days unless rain and/or snow occurs during the short period of time—particularly for bare soils in arid and semi-arid environments, for which the surface of the ground is normally dry (Kerr et al., 1992). (2) Atmospheric radiative transfer simulations show that in clear-sky conditions the surface-reflected diffuse solar irradiance term is much smaller than the surface-reflected solar beam term in the thermal infrared range, and the surface-reflected atmospheric downward thermal irradiance term is smaller than surface thermal emission. So the Lambertian approximation of the surface reflection does not introduce significant error in the 3–14 μm thermal infrared region. Then we can link hemispherical directional reflectance $r(\theta)$ to directional emissivity $\varepsilon(\theta)$ by $r(\theta) = 1 - \varepsilon(\theta)$ according to Kirch-

hoff's law. Based on the above assumptions, the radiance measured in MODIS band j can be expressed as

$$L_j = t_{j,1}\varepsilon_j B_j(T_s) + L_{j,a} + L_{j,s} + \frac{1 - \varepsilon_j}{\pi} [t_{j,2}\alpha\mu_0 E_{j,0} + t_{j,3}E_{j,d} + t_{j,4}E_{j,t}], \quad (3)$$

where all terms are band-averaged, ε_j is the surface emissivity, $B_j(T_s)$ is the radiance emitted by a blackbody at surface temperature T_s , $L_{j,a}$ is the thermal path radiance, $L_{j,s}$ is the path radiance resulting from scattering of solar radiation, and $E_{j,0}$ is the spectral solar irradiance incident on the top of the atmosphere (normal to the beam). $E_{j,d}$ and $E_{j,t}$ are the band-averaged solar diffuse irradiance and atmospheric downward thermal irradiance at the surface, and $t_{j,i}$, $i=1, \dots, 4$ are the band effective transmission functions weighted by the band response function, the corresponding radiance, and irradiance terms. Note that we have neglected the in-band spectral variation of the surface emissivity in reducing a general integral equation into Eq. (3), and have omitted symbols of view angle and solar angle for most terms in the above equation. On the right-hand side of this equation, ε_j , α , and $B_j(T_s)$ depend on surface properties and conditions. All other terms depend on atmospheric water vapor and temperature profiles, solar angle and viewing angle. These terms can be given by numerical simulations of atmospheric radiative transfer. The set of 14 nonlinear equations in the day/night algorithm is solved with the least-squares fit method (Wan & Li, 1997).

Considering the angular variation in surface emissivity, we separate the whole range of MODIS viewing zenith angle into sub-ranges, and use one emissivity in each of the sub-ranges. In the day/night LST processing, we select a pair of clear-sky daytime and night MODIS observations at view angles in a same sub-range whenever it is possible. If there is no such pair of day/night observations available in a reasonable short period of time but there is a pair of day/night observations in different sub-ranges of view angle, we use this less favorable pair for surface emissivity and temperature retrieval and set a lower quality for the retrieved results. Sometimes we have to make a tradeoff between a favorable period of time and a favorable pair of view angles for temporal variations versus angular variations in surface emissivities. If the time difference between daytime and nighttime observations is too long, the chance for a large change in surface emissivity will be high. In the new product generation executive (PGE) code (version 3), the whole range of MODIS viewing zenith angle is separated into four sub-ranges (0–40°, 40–52°, 52–60° and 60–65°, respectively), instead of two sub-ranges in the earlier versions.

4. Performance of MODIS TIR bands

The specification and estimated performance of the TIR bands in the MODIS Proto-Flight Model (PFM) flown on

Terra are shown in Table 1. The channel-dependent noise and systematic error in MODIS TIR channel data were evaluated with early MODIS data over lake and ocean sites in clear-sky days acquired with the A-side of scan mirror and electronics before the end of October 2000 (Wan, 2002). In 14 cases of sub-area sites with a size of 10 lines by 16 pixels each line, where the brightness temperature in band 31 changes within ± 0.1 K, average and standard deviation values of brightness temperatures in 10 channels (consisting a 10-element linear detector array) of 16 MODIS TIR bands show the channel-dependent noise and systematic errors. It is found that the ninth channel in bands 21 and 24, and the fourth channel in band 22 are too noisy to use, and that the specification of noise equivalent temperature difference (NEDT) is reached in all other channels of the 16 MODIS TIR bands. There are significant channel-dependent systematic errors in 1–3 channels in bands 22, 23, 25, 27–30. After a simple correction of the channel-dependent systematic errors with the statistics in the above 14 cases, the quality of the MODIS TIR data is significantly improved in bands 22–25, and 27–30, and the NEDT specification is reached or nearly reached in all bands as shown in column 5 of Table 1.

The absolute radiometric accuracy of MODIS TIR channel data was evaluated with in situ data collected in a vicarious calibration field campaign conducted in Lake Titicaca, Bolivia, during May 26 and June 17, 2000 (Wan et al., 2002). The comparison between MODIS TIR data produced by the new Level-1B code (version 2.5.4) and the band radiances calculated with atmospheric radiative transfer code MODTRAN4.0 (Berk et al., 1999) based on lake surface temperatures measured by five IR radiometers deployed in the high-elevation Lake Titicaca, and the atmospheric temperature and water vapor profiles measured by radiosondes launched on the lake-shore on and June 13

and 15, 2000, calm clear-sky days, shows good agreements in bands 29, 31 and 32 (within an accuracy of 0.5%) in daytime overpass cases. Sensitivity analysis indicates that the changes on the measured atmospheric temperature and water vapor profiles result in negligible or small effects on the calculated radiances in bands 20–23, 29, and 31–32. Therefore, comparisons for these bands were made for cases when lake surface temperature measurements were available but no radiosonde data were available, and in sub-areas of 10×16 pixels where there was no in situ measurement but MODIS brightness temperatures in band 31 vary within ± 0.15 K by using the validated band 31 to determine lake surface temperatures. These comparisons show that the specified absolute radiometric accuracy of 1% is reached or nearly reached in MODIS bands 21, 29, and 31–33, and that there is a calibration bias of 2–3% in bands 20, 22, and 23. The error analysis also shows that the radiosondes cannot provide accurate atmospheric temperature and water vapor profiles to estimate the calibration accuracies in the atmospheric sounding bands at the specified 1% level and that the calibration accuracy in the ozone band (band 30) cannot be estimated without in situ measurements of ozone. Column 6 in Table 1 shows the estimated values of calibration bias, which are averaged from sub-areas with viewing zenith angles smaller than 50° in June 13 and 15.

The MODIS sensor was reconfigured on October 31 and November 1, 2000, to the B-side Science Mode from the A-side Science Mode (see Terra PFM Instrument Status and Terra MODIS History on webpage <http://mcstweb.gsfc.nasa.gov/Home.html>). By transiting to latest focal plane bias voltage in the B-side configuration, the three originally noisy detector elements returned to normal performance. The MODIS instrument experienced a Power Supply 2 shutdown anomaly and did not take science data during the time period of June 15 to July 2, 2001. The MODIS instrument was

Table 1

Specifications of the Terra MODIS TIR bands, and its estimated performance in the A-side configuration before October 31, 2000 (Wan et al., 2002) and the new A-side configuration after July 3, 2001

Band	Bandwidth (μm)	IFOV	NEDT (K)		Calibration bias estimated (K) (before October 31, 2000)	Calibration bias estimated (K) (after July 3, 2001)
			Specified	Estimated (Wan, 2002)		
20	3.660–3.840	1 km	0.05	0.06	0.60	0.63
21	3.929–3.989	1 km	2.00	0.64	0.46	0.70
22	3.929–3.989	1 km	0.07	0.07	0.55	0.15
23	4.020–4.080	1 km	0.07	0.05	0.40	–0.18
24	4.433–4.498	1 km	0.25	0.13		
25	4.482–4.549	1 km	0.25	0.08		
27	6.535–6.895	1 km	0.25	0.12		
28	7.175–7.475	1 km	0.25	0.09		
29	8.400–8.700	1 km	0.05	0.03	0.03	–0.12
30	9.580–9.880	1 km	0.25	0.08		
31	10.780–11.280	1 km	0.05	0.03	0.12	0.09
32	11.770–12.270	1 km	0.05	0.05	–0.19	0.05
33	13.185–13.485	1 km	0.25	0.16	0.55	(0.98)
34	13.485–13.785	1 km	0.25	0.27		
35	13.785–14.085	1 km	0.25	0.23		
36	14.085–14.385	1 km	0.35	0.41		

reconfigured to the A-side Science Mode with the same focal plane bias voltage used in the B-side mode on July 3, 2001. The MODIS data in this configuration are referred as new A-side data. To evaluate the calibration accuracy of the new A-side data, we conducted a field campaign in Walker Lake, Nevada (NV) in mid-October 2001. The size of Walker Lake is approximately 20 km long in the S–N direction and 7 km wide in the E–W direction. The lake surface elevation is 1196 m above sea level. On October 18, 2001, a clear-sky day, the lake surface temperature was measured by four TIR radiometers located around 38.69721°N and 118.70802°W. After correcting the effect of lake surface emissivity, the measured lake surface temperature is 290.56 K (with a standard deviation of 0.07 K in the four sets of measurements). The column water vapor calculated from the atmospheric profile measured by radiosonde is 0.95 cm. Following the same procedures used in the Lake Titicaca vicarious field campaign (Wan et al., 2002), we estimated the calibration bias in the new A-side TIR data, as shown in column 7 of Table 1. The root sum squares of uncertainties in the calibration accuracy estimate is about 0.3 K for bands 20, 22–23, 29, and 31–32, and 0.8 K for bands 21 and 33.

As shown in columns 4 and 5 of Table 1, MODIS bands 31 and 32, which are used to retrieve LST with the generalized split-window algorithm, meet the NEDT specification. The effects of calibration bias in these two bands on the LST algorithm depend on the resulting errors in the average and difference of brightness temperatures in these two bands, i.e., errors in $0.5(T_{31} + T_{32})$ and $0.5(T_{31} - T_{32})$. The error in the first term caused by the calibration bias in both old and new A-side data is less than 0.1 K. In the old A-side data, the error in the second term is around 0.3 K, introducing an error of 0.5 K or slightly larger to the retrieved LST. Although this amount of error is too large for SST to meet its accuracy specification of 0.3–0.5 K, it is considered marginal for LST to meet the 1 K accuracy specification. For the new A-side data, the error in the second term is much smaller. The estimated performance of bands 20, 22–23, 29, and 31–33, which are used in the MODIS day/night LST algorithm, shows that NEDT meets the specifications in all these bands, and that the calibration bias is small for longwave bands but is about 2–3% of the radiance in the three mid-wave bands for the old A-side data. For the new A-side data, the calibration bias is less than 1% in bands 22–23, 29, and 31–32.

5. MODIS LST products

5.1. A brief description

The MODIS LST data products are produced in a sequence. The sequence begins in a swath (scene) of MODIS data at a nominal pixel spatial resolution of 1 km at nadir and a nominal swath coverage of 2030 or 2040 lines (along track, about 5 min of MODIS scans) by 1354 pixels

per line. The first product, MOD11_L2, is an LST product at 1-km spatial resolution for a swath. This product is the result of the generalized split-window LST algorithm (Wan & Dozier, 1996). The second product, MOD11A1, is a tile of daily LST product at 1-km spatial resolution (the exact grid size is 0.927 km, or 0.5 arc-min at the equator). It is generated by mapping the pixels from the MOD11_L2 products for a day to the Earth locations on the integerized sinusoidal projection. The third product, MOD11B1, is a tile of daily LST and emissivities at 5-km spatial resolution (the exact grid size is 4.633 km or 2.5 arc-min at the equator). It is generated by the day/night LST algorithm (Wan & Li, 1997). The fourth product, MOD11A2, is for the 8-day LST produced by averaging the MOD11A1 product in a period of 8 days. Other LST products are the daily, 8-day, and monthly global LST products in a geographic projection at the 0.25° spatial resolution of the Climate Modeling Grid (CMG) cells. They are derived from the MOD11A1 and MOD11B1 daily LST products.

The level-2 LST product, MOD11_L2, is generated using the MODIS sensor radiance data product (MOD021KM), the geolocation product (MOD03), the cloud mask product (MOD35_L2), the atmospheric temperature and water vapor product (MOD07_L2), the quarterly land-cover (MOD12Q1), and snow product (MOD10_L2). For complete global coverage, the MOD11_L2 LST product is generated for all swaths acquired in daytime and nighttime on the Earth including the polar regions. This MOD11_L2 LST product contains nine scientific data sets (SDSs): LST, QC for quality assurance (QA) control, Error_LST, Emis_31, Emis_32, View_angle, View_time, Latitude, and Longitude. The first seven SDSs are for 1-km pixels. The last two SDSs are coarse resolution (5 km) latitude and longitude data. Each set corresponds to a center pixel of a block of 5×5 pixels in the LST SDS. For effective use of the space, the QC SDS uses 16 bits to store eight flags. Bits 00–01 are used for the Mandatory QA flags which is defined by the MODIS Land group: 00 stands for a pixel in which LST is produced in good quality, not necessary to examine more detailed QA bits; 01 for a pixel with LST produced in unreliable or unquantifiable quality, recommend examination of more detailed QA bits; 10 for a pixel not produced due to cloud effects (note that LST is produced only for pixels in clear-sky conditions at the 99% confidence); 11 for a pixel not produced primarily due to reasons other than cloud (for example, in ocean). Note that Fill Value 0 is not the fill value for the whole QC SDS. It is used only for the other seven flags. Therefore, the QC SDS should be used together with the LST SDS: for pixels with Fill Value 0 in the LST SDS, all the other seven flags in the QC SDS are given a fill value; the values in the other seven flags represent meaningful information related to the LST quality only for pixels with non-zero values (specifically, zero in the other seven flags means the best quality in LST).

The product generation executive (PGE) code for the daily MODIS LST products, PGE16, consists of two proc-

ess segments: MOD_PR11A1 and MOD_PR11B1. The MOD_PR11A1 process generates LSTs in the MOD11_L2 product for all clear-sky pixels at a 99% confidence defined by MOD35_L2, and maps the LSTs to the 1-km grids in the level-3 MOD11A1 product. The MOD_PR11A1 also accumulates all useful information into the interim products (MOD11UPD) in the 5-km tiles, including radiance values in the seven bands used in the day/night LST algorithm which are contributed from clear-sky pixels, viewing angles and solar angles, and related information from the atmospheric profile. Based on the information in MOD11UPD, the MOD_PR11B1 process generates the LST and emissivity values with the day/night LST method at 5-km resolution grids in the MOD11B1 product. Two new SDSs (LST_Day_5km_Aggregated_from_1km and LST_Night_5km_Aggregated_from_1km) are also included in the MOD11B1 product to store the LST values aggregated from the LST_Day_1km and LST_Night_1km data in the MOD11A1 product. These two SDSs have been used to produce the quick looks of the LST product in the MODIS Land Global Browse web page <http://modland.nascom.nasa.gov/browse>).

5.2. A double-screen scheme to remove cloud-contaminated LSTs

Although the state-of-the-art techniques based on multiple MODIS bands have been used in the MODIS cloud mask product (MOD35_L2), and the MODIS LST PGE produces LSTs only for the clear-sky pixels at the highest confidence (99%) defined by MOD35_L2, there are still some small possibilities that MODIS LSTs are contaminated with cloud effects because of the difficulty to accurately discriminate true clear-sky pixels from cloud pixels and pixels contaminated with sub-pixel clouds. The quality assurance provided in the MODIS LST products at the pixel or grid levels is based on the quality information in the input products and the knowledge obtained from error analysis of LST algorithms in clear-sky conditions. Therefore, it is impossible to make the confidence of the quality assurance in the MODIS LST products higher than 99%.

The simulations of LST algorithms indicate that the difference in the LSTs retrieved by the day/night LST method and the LSTs retrieved by the generalized split-window LST method in clear-sky conditions depends on the uncertainties in the classification-based emissivities and the column water vapor, and it ranges from a few minus degrees to 10 K at most. But the range of difference calculated from the real MODIS LST products in large regions is sometimes much wide due to the different sensitivities of the two LST algorithms to the cloud effects. We propose the use of this LST difference statistics to remove the LST values that are contaminated with cloud effects: screening off 1% of both the daytime and nighttime LSTs by the upper and lower ends of the LST difference distributions. Fig. 1 shows the histograms of the LST differences over the North America

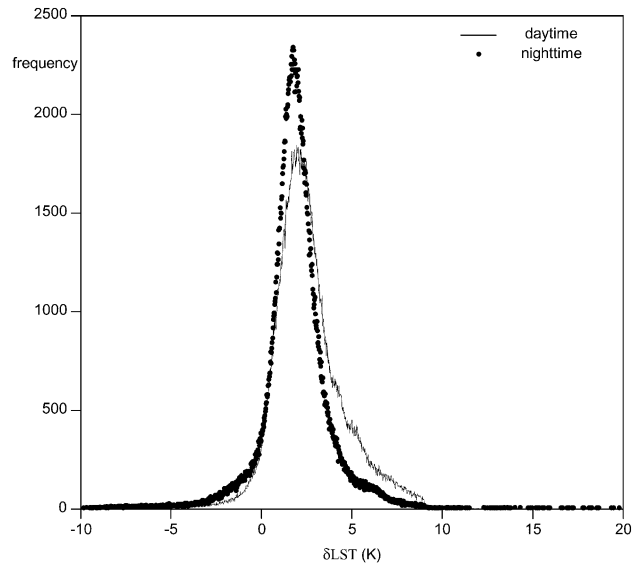
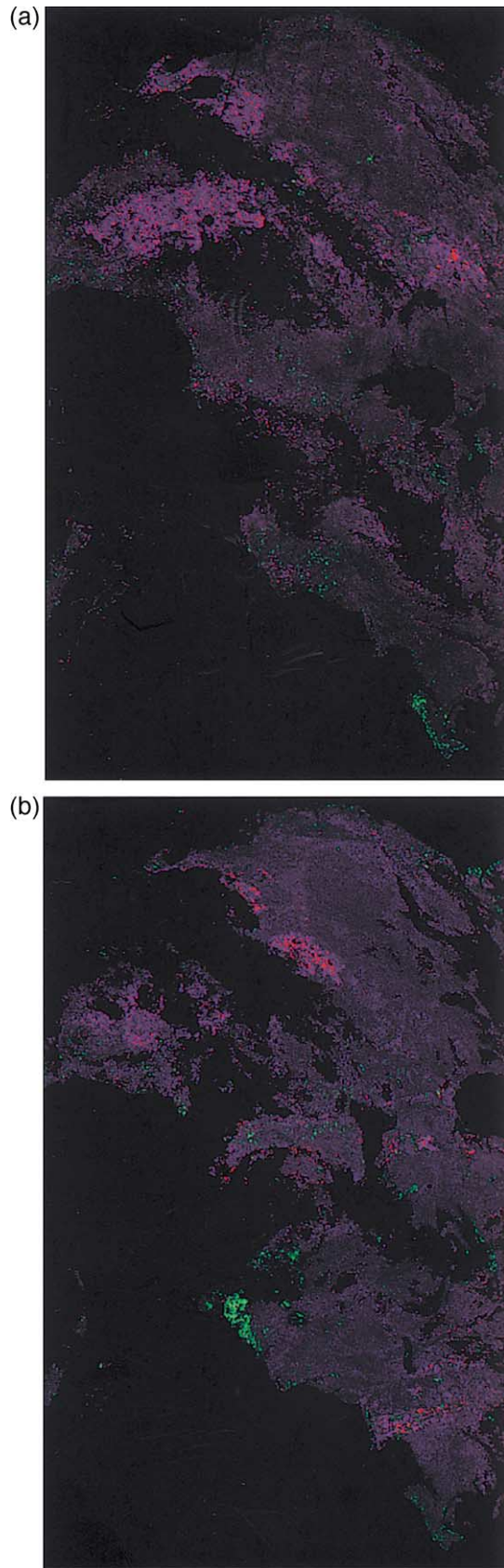


Fig. 1. Histograms of the difference between the 5- and 1-km LSTs over the North America Continent between latitudes 20° and 50° on July 21, 2001.

Continent between latitudes 20° and 50° on 21 July 2001. Fig. 2 shows the images of daytime (a) and nighttime (b) LST differences, over the same region on the same day. Fig. 3 shows the 5-km daytime and nighttime LSTs, and the band emissivities in the 8-day period of July 20–27, 2001. In the color composite image in Fig. 2(a), the red component represents the positive portion of the daytime LST difference in such a way that the grids screened off are at grey level of 255 and the remaining grids are in the grey scale of 15–215, the green component represents the negative portion of the daytime LST difference in a similar way, and the blue component is the LST difference itself in the grey scale of 15–255. The same applies for the nighttime LST difference in Fig. 2(b). Therefore, the points in brightest red represent the grids screened off because their LST differences are too large in the positive direction, and points in the brightest green represent the grids screened off because their LST differences are too large in the negative direction. We can see that most of these screened grids in the brightest red and green are by the edges of the LST difference image (the blue component), i.e., they are close to the areas covered by clouds. Such a distribution of the screened grids justified this screen scheme proposed to remove the cloud-contaminated LSTs. Before the screening, the daytime LST difference ranges from -15 to 22 K and the nighttime LST difference ranges from -26 to 35 K. After the screening, the LST difference range reduces to -1.96 to 8.24 K for the daytime and -3.36 to 6.84 K for the nighttime. The averaged LST differences are 2.62 and 1.91 K for the daytime and nighttime LSTs, respectively. The averaged LST differences are different because the daytime and nighttime LSTs are distributed in different areas and in the daytime LST image there are more clear-sky grids in the semi-arid and arid midwest regions where surface emissivities have lower values. The difference



between the LSTs retrieved from the day/night method and the LSTs retrieved from the split-window method reveals that the classification-based emissivities used in the split-

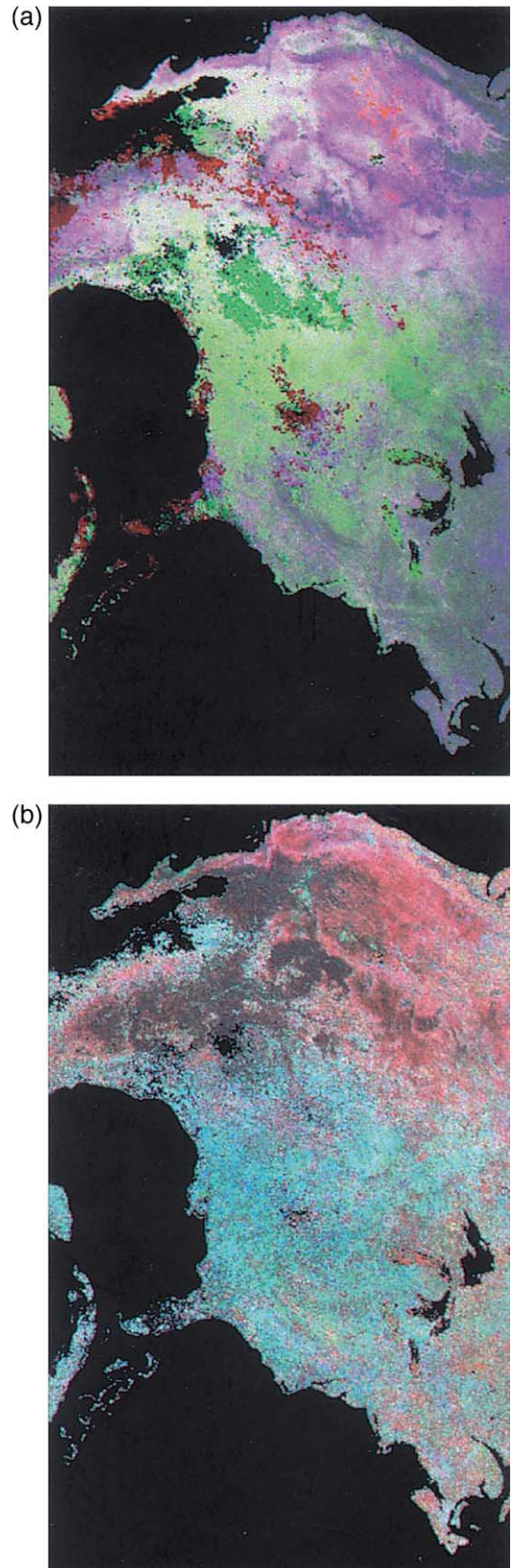


Fig. 2. Color composite images of daytime (a) and nighttime (b) LST differences over the same region on the same day as in Fig. 1. Read text for details of the RGB components.

window LST method are overestimated, especially in the semi-arid and arid regions. In the second step of the proposed double-screen scheme, the histogram of difference between daytime and nighttime LSTs is used to remove the grids contaminated with cloud effects after the first screen described above: screen off 0.5% of the daytime and nighttime LST pairs by the upper and lower ends of the LST difference distribution. Fig. 3 shows the 5-km daytime and nighttime LSTs, and the band emissivities in the 8-day period of July 20–27, 2001, for the same region as in Fig. 2. In Fig. 3(a), the red (R), green (G), and blue (B) components represent the histogram-enhanced daytime, nighttime LSTs and the day/night LST difference after screening out the cloud-contaminated grids with the double-screen scheme. The points in brightest red represent the grids without nighttime LSTs and the points in brightest green represent the grids without daytime LSTs because of clouds. A complete coverage of the LST and surface emissivities can be obtained with more days of data. In Fig. 3(b), the RGB components represent the emissivities in MODIS bands 29, 22, and 20 enhanced with the histogram equalization method, respectively. Because all the RGB components in Fig. 3 have been enhanced with the histogram equalization method in order to clearly present the spatial contrasts, there is no simple way to show the color scales of the color composite images. Instead, temperature and emissivity ranges are listed for the RGB components in the figure caption. The spatial features in the daytime and nighttime LSTs, the day/night LST, and the band emissivities show the great potentials of the 5-km MODIS LST product in various applications.

6. Validation results

The MODIS LST algorithms were validated with MAS data collected in several field campaigns since the field campaign conducted over a silt playa in Railroad Valley, NV, in June 1997 (Snyder, Wan, Zhang, & Feng, 1997). According to the experience gained in our field campaigns, the major sources of uncertainties in the LST validation are the spatial variations in surface temperature and emissivity within an MAS or MODIS pixel. When these spatial variations are significantly large, it will not be possible to accurately measure the surface temperature at the scale of pixel size with ground-based instruments. The key requirements for a good site of LST validation are: its size being large enough to cover at least dozens of MODIS pixels,

homogeneous surface materials and emissivity and temperature, its easy accessibility for the deployment of instruments, and less interference between the validation activities and the normal life activities.

In order to validate the MODIS LST product, we conducted three field campaigns in 2000 and four field campaigns in 2001 in California (CA) and Nevada (NV), in addition to the vicarious calibration field campaign conducted in Lake Titicaca, Bolivia, in May/June 2000. The field campaigns conducted in 2000 include early April in Mono Lake and Bridgeport grassland in CA, late July in Railroad Valley, NV, and in Mono Lake, Bridgeport grassland and a rice field in Chico, CA, and early October in Mono Lake and Bridgeport, CA. The field campaigns conducted in 2001 include March–April in Bridgeport, CA and Walker Lake, NV, mid-late July in Railroad Valley, NV, and in Mono Lake and Bridgeport, CA, August in Mono Lake and Bridgeport, CA, and October in Walker Lake, NV, and Bridgeport, CA. Each field campaign lasted for 2–3 weeks to cover a flight opportunity window of the MODIS Airborne Simulator (MAS).

6.1. Validation of the 1-km level-2 LST product using lake sites

We selected lake sites as our primary sites for LST validation in the first 2 years of MODIS LST production because of the following considerations. Because water surface emissivity can be accurately calculated from refractive index and surface temperature is often much more uniform in lakes than other land sites, lake surface radiometric temperature at a scale of 1-km may be accurately measured by IR radiometers at multiple locations in most cases. We know that the uncertainty in surface emissivities in MODIS bands 31 and 32, and the residual error in LST after correcting the atmospheric effects with the split-window method are the only two major error sources in the level-2 1-km MODIS LST product (MOD11_L2). We can reduce the emissivity-related error source to minimal with lakes as validation sites so that the residual error related to atmospheric corrections in the LST algorithm can be estimated by the difference between measured lake surface temperatures and the values in the MODIS LST product. If the surface temperature values in the MODIS LST product agree well with the measured lake surface temperatures in lake sites in different seasons, this will validate the capability of the MODIS LST algorithm in atmospheric effect corrections. Once an estimate of the atmospheric-correction related residual error is obtained, we can apply this estimate to MODIS LST values in other locations, where it may be difficult or even impossible to make accurate in situ measurements of surface temperatures at the 1-km scale because of terrain and spatial variations in LST. In this way, we can indirectly validate the MODIS LST product in non-lake areas where the surface emissivities in bands 31 and 32 can also be well estimated from the land cover types and

Fig. 3. (a) Color composite image with the 5-km daytime LSTs (in the range of 255.1–335 K), nighttime LSTs (243.9–310.8 K), and their difference (–0.92 to 37.1 K) as RGB components, and (b) color composite image with the band emissivities in bands 29, 22, and 20 (in ranges of 0.670–0.996, 0.638–0.996, and 0.662–0.996, respectively) as RGB components, in the 8-day period of July 20–27, 2001.

viewing angle, such as in vegetated areas. If we can make accurate ground-based measurements of lake surface temperature and atmospheric profile in dry atmospheric condition, the in situ measurement data can also be used to evaluate the calibration accuracy of MODIS TIR bands in the atmospheric windows. We selected Mono Lake and Waker Lake as our primary LST validation sites also because of the relative short distance between the sites and the UCSB campus and the distance between the sites and the aircraft base (Dryden Flight Research Center) for the MAS instrument so that we can arrange our field campaigns more flexibly and efficiently. We can drive to the sites from Santa Barbara with all ground-based instruments in two vehicles in a single day. It is possible to fly daytime and nighttime MAS missions in a single day when it is in good weather conditions. Mono Lake has a relatively large open water area in its eastern portion, approximately 13 km in the S–N direction and 9 km in the E–W direction. This portion will be covered by around 100 MODIS pixels. The elevation of Mono Lake is 1945 m above sea level. Walker Lake has a size of approximately 20 × 7 km, at 1196 m above sea level.

Lake Titicaca is a very good validation site for the TIR absolute radiances because it is a high elevation (3841 m above sea level) lake located in a large plateau in South America and it has a large size of open water surface (8100 km²).

The same TIR radiometers and radiosonde system that were used in our vicarious calibration field campaign conducted in Lake Titicaca in June 2000 were also used in our LST validation field campaigns. The detailed technical specifications and real performance qualities and the procedures to correct the effect of surface emissivity on the measured surface temperature can be found in the MODIS calibration paper (Wan et al., 2002). The accuracy of the IR radiometers is better than 0.2 K.

On April 4, 2000, a clear-sky day, four IR-radiometer floating systems were deployed in Mono Lake. The averaged value of lake surface kinetic temperatures measured by the IR radiometers at the MODIS overpass time is 283.81 K with a standard deviation of 0.52 K, as shown in columns 7 and 8 of case 1 in Table 2. The averaged latitude and longitude values of the IR radiometers positions are given in column 3. Date and overpass time of the Terra MODIS are given in column 4. The zenith and azimuth angles of the MODIS observation are given in column 5. In column 6, the atmospheric column water vapor (cwv) in the upper line comes from MOD07_L2 and that in the lower line comes from radiosonde. Because we have only one radiosonde system, we cannot measure the atmospheric temperature and water vapor profile at each site when we make in situ measurements with IR radiometers in multiple sites at the same time. The version number of the MODIS level 1B data is given in column 9. The MODIS LST value, which in general is interpolated from the MOD11_L2 LST values at four pixels neighboring the averaged position of IR radiometers, is given in column 10. The difference between the

Table 2
Comparison between the 1-km MODIS LSTs and in situ measured LSTs in validation field campaigns conducted in 2000 and 2001

Case no.	Site	Latitude, longitude	Date (month/day/year), time	View zenith azimuth (°)	Atmos. cwv (cm)	In situ T _s from radiometers (K) (no.)	Spatial variation ΔT _s (K)	MODIS LIB version	MODIS T _s (ΔT _s) (K)	MODIS – in situ T _s (K)
1	Mono Lake, CA	37.9712°N, 119.0014°W	4/04/00, 11:19 PST	22.38, –78.35	2.2 (0.36)	283.81 (4)	0.52	2.4.2	284.7 (0.2)	+0.9
2	Mono Lake, CA	37.9930°N, 118.9646°W	7/25/00, 11:18 PST	22.09, –79.37	2.1	296.01 (3)	0.15	2.5.4	296.3 (0.2)	+0.3
3	Mono Lake, CA	38.0105°N, 118.9695°W	10/06/00, 11:11 PST	11.35, –78.19	1.4 (0.62)	290.17 (4)	0.23	2.4.3	290.4 (0.1)	+0.2
4	Lake Titicaca, Bolivia	16.2470°S, 68.7230°W	6/15/00, 15:26 UTC	34.3, –82.7	1.1 (0.29)	285.0 (5)	0.3	2.5.4	285.5 (0.5)	+0.5
5	Walker Lake, NV	38.6972°N, 118.70802°W	10/18/01, 10:57 PST	0.74, –100.23	0.81 (0.95)	290.56 (4)	0.1	3.0.0	290.74 (0.2)	+0.2
6	Bridgeport, CA	38.2255°N, 119.2680°W	4/04/00, 11:19 PST	20.00, –79.38	2.6	308.2 (4)	0.9	2.4.2	307.3 (2.3)	–0.9
7	Bridgeport grassland	38.2202°N, 119.2693°W	7/27/00, 22:09 PST	11.81, 81.33	1.6	281.63 (4)	0.6	2.5.4	282.4 (0.4)	+0.8
8	Bridgeport grassland	38.2202°N, 119.2693°W	7/29/00, 21:57 PST	32.36, 77.56	2.4	283.24 (4)	0.6	2.5.4	283.0 (0.2)	–0.2
9	Rice field California	39.5073°N, 121.8107°W	7/27/00, 22:10 PST	26.1, 77.3	1.4	291.20 (1)		2.5.4	292.1 (0.5)	+0.9
10	Rice field California	39.5073°N, 121.8107°W	7/29/00, 21:57 PST	42.67, 75.8	3.0	293.02 (1)		2.5.4	292.9 (0.8)	–0.1
11	Bridgeport snowcover	38.2199°N, 119.2683°W	3/11/01, 22:36 PST	40.48, –97.32	0.4	263.70 (2)	(0.2)	3.0.0	263.7 (0.2)	+0.0

The atmospheric column water (cwv) value from MOD07_L2 is followed by the value from radiosonde in the parentheses. Most MOD11_L2 LSTs are retrieved from LIB data in version 2.5.4 or later except cases 1, 3 and 6.

MODIS LST value and the LST value from in situ measurements is given in the last column. In case 1, we cannot apply the 4-pixel interpolation because the positions of two IR radiometers are too close to Paoha Island in the middle of the lake. Therefore, we shifted the averaged position to the east by 1 km in this case only. The difference between the MODIS T_s value and the averaged in situ measured lake surface temperature is 0.9 K in this case. There are two reasons for this relatively large difference value: (1) MODIS level 1B data is in version 2.4.2 in this case so that the band 31 radiance has an error up to 0.5%; (2) the value of atmospheric column water vapor given by MOD07_L2 in its early version is 2.2 cm, which is much larger than the value of 0.36 cm calculated from the atmospheric humidity profile measured by radiosonde.

The next case is also for Mono Lake in the July field campaign. On July 25, we got good measurement data from only three IR radiometers and others had problems with the batteries. The IR radiometers were deployed far away from the lake shore. The averaged lake surface temperature measured by the IR radiometers is 296.01 K with a standard deviation 0.15 K. The MODIS LST calculated from MODIS L1B data in v2.5.4 is only 0.3 K larger than the in situ value. Note that MODIS L1B data in version 2.5.4 or later give right radiance values in TIR bands (details are available in the version history file at the MODIS Calibration Support Team home page <http://mcstweb.gsfc.nasa.gov/Home.html>). In case 3, four IR radiometers were deployed all in the

middle of the open water area on 6 October 2000. The MODIS LST value is larger than in the situ value by 0.2 K.

Case 4 is for the field campaign conducted in Lake Titicaca, Bolivia, on June 15, 2000. Five IR radiometers were deployed in this case. The MODIS LST value is larger than the in situ value by 0.5 K. Details are given in Wan et al. (2002).

Case 5 is for the field campaign conducted in Walker Lake, NV, on October 18, 2001. The MODIS LST value, which is retrieved from the new A-side MODIS data in v3.0.0, is larger than the in situ value by 0.2 K.

As shown in the last column in the five cases of lake sites in Table 2, the differences between LST values from the MODIS LST product and the in situ measured LST values range from 0.2 to 0.9 K. Except for the first case in which there is a known error of up to 0.5% in the MODIS band 31 data, the differences between MODIS and in situ LSTs are in the same level of the IR radiometer accuracy and the spatial variations in surface temperatures measured by IR radiometers and MODIS. The uncertainties related to the IR radiometer, spatial variations in the in situ measured temperatures (i.e., the standard deviation divided by the square root of the total number of the IR radiometers) and in the MODIS measured temperature do not exceed 0.2, 0.13, and 0.5 K, respectively. The root sum square (RRS) of all these three uncertainties is 0.55 K. Therefore, we got the estimate of the residual error after atmospheric effect corrections in the 1-km MODIS LST product, which is approximately 0.6 K.

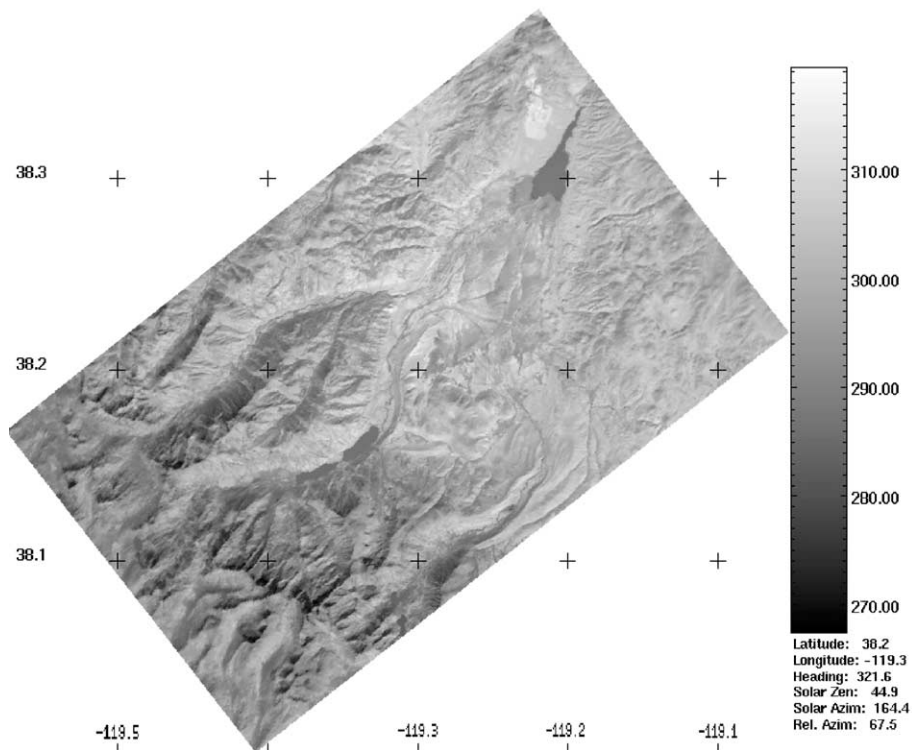


Fig. 4. Brightness temperature image calculated from band 45 radiance (centered at 10.95 μm) of MAS data collected over Bridgeport, CA, on October 6, 2000.

6.2. Validation of the 1-km level-2 LST product using vegetation sites

The same supporting structure used in the floating system for the IR radiometer was also used in the field campaign conducted in the Bridgeport grassland in early April 2000 just before the flood-irrigation started on April 15, giving an instant-field-of-view (IFOV) of 32 cm in diameter on the grassland surface. Because there was no cattle and horse grazing on the grassland during the field campaign, we were allowed to deploy four IR radiometers in the middle of a grassland owned by Hunewill Circle H Ranch. The four IR radiometers were placed at the corners of a rectangle with a length of 50 m each side with the hope that the measured surface temperatures can be compared to MAS data. Unfortunately, there was no MAS flight over the Mono Lake and Bridgeport area until October 2000 because of technical and schedule problems. At the beginning, one IR radiometer was intentionally deployed at a location where soil surface was wetter than other locations. The differences in the surface temperatures measured by the IR radiometers were up to 7 K in daytime data and 5 K in nighttime data around the MODIS overpass time. After we moved the IR radiometers into an area where grass was more uniform and there is no obvious

difference in the soil surface moisture conditions, the maximum difference was still around 2 K. The MODIS LST value is smaller than the in situ value by 0.9 K. Because of the large variation in measured surface temperatures and the MODIS L1B data in v2.4.2, we should give less weight for this case (case 6).

Fig. 4 shows the brightness temperature image calculated from band 45 radiance (centered at $10.95 \mu\text{m}$) of MAS data collected over Bridgeport, CA, on October 6, 2000. We can verify the large spatial variation in daytime LSTs with this MAS image by showing brightness temperature values of some MAS pixels (with the size of approximately 50 m) by the location of our measurements: 305.7 K at the pixel in line 362 sample 472 (latitude 38.225° , longitude -119.268°), 312.1 K at the pixel in line 369 sample 468 (latitude 38.225° , longitude -119.271°), and 300.3 K at the pixel in line 351 sample 465 (latitude 38.220° , longitude 119.268°). The distance between the first two pixels is 403 m and the third pixel is 652 m away from the first pixel. These numbers show the difficulty for the in situ measurements of daytime LSTs and the great advantage of the thermal infrared remote sensing with MODIS in providing the global LST distribution at 1-km resolution in clear-sky conditions in cases where it is difficult to make in situ measurements.

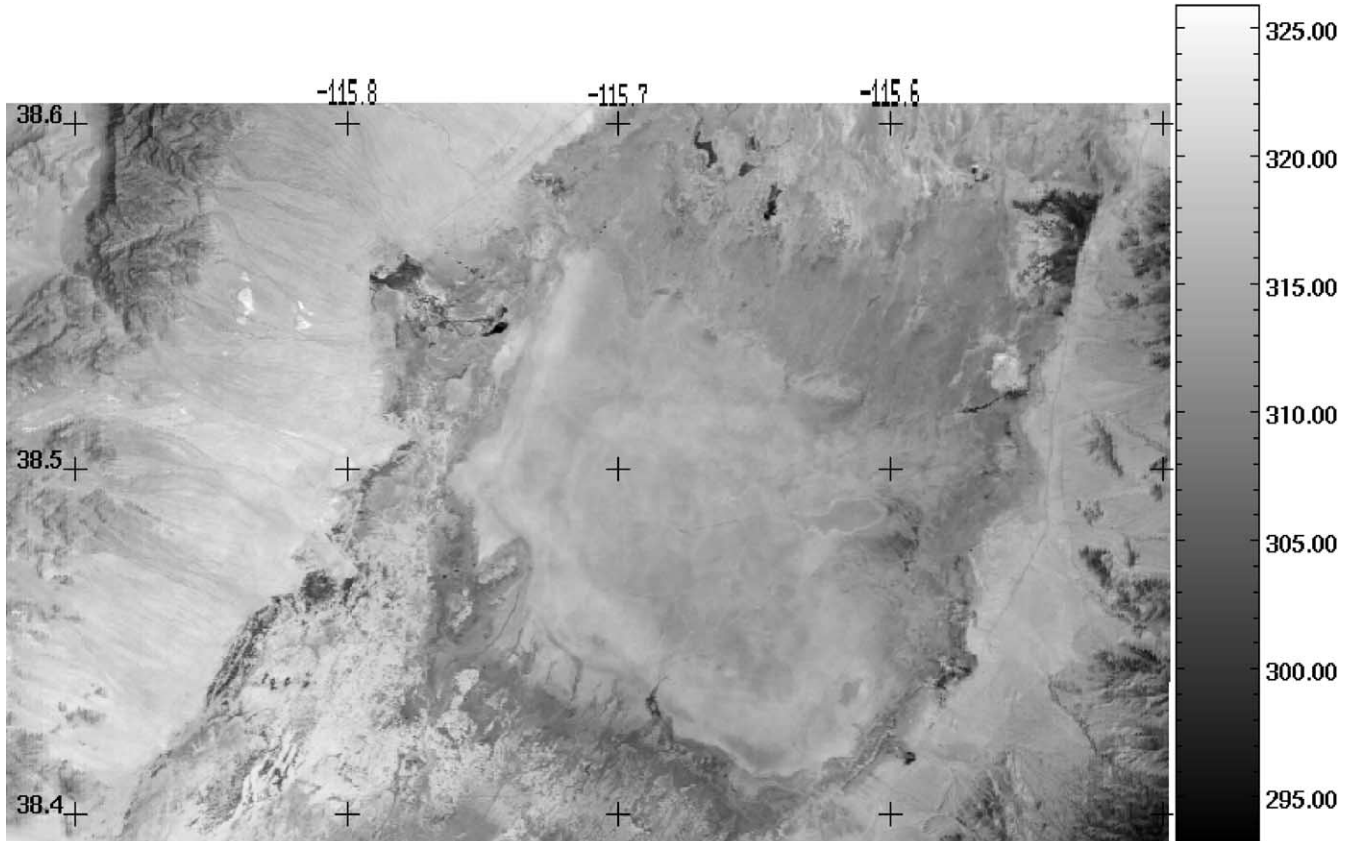


Fig. 5. Brightness temperature image calculated from band 45 radiance (centered at $10.95 \mu\text{m}$) of MAS data collected over Railroad Valley, NV, on June 23, 1997.

After the Bridgeport field campaign in April 2000, we designed a better strategy for measuring nighttime LST in grassland. During the late July field campaign, the Bridgeport grassland was irrigated, and there were cattle and horses grazing in the field. Instead of using the plastic supporting systems for the IR radiometers in the field, we set two poles by the edge of the grassland and fixed one IR radiometer at the top of each pole. The IR radiometer viewed toward the grassland surface at approximately 3.5 m above ground, with IFOV of 1.5 m in diameter. On the nights of July 27 and 29, two persons—each carrying one IR radiometer—walked back and forth along two almost parallel transects in the middle of the grassland under the clear-sky moon lights for more than 1 h covering the MODIS nighttime overpass times. We averaged the measured surface temperatures along the transects and found that the averaged values are compatible to the values measured by the IR radiometers on the poles. The results for these two nights are listed as cases 7 and 8 in Table 2.

During the late July field campaign, we also set one pole for an IR radiometer in the middle of a rice field in Chico, CA, which is a test site used by Dr. Richard E. Plant, University of California at Davis. Because a series of rice fields with the size of approximately 50 × 50 m each are distributed in the area, there are only narrow roads and irrigation canals between them, and there is no large difference between the surface temperatures over rice canopy and roads at night, we believe that the surface temperature measured by a single IR radiometer is still useful for the validation of nighttime MODIS LST product. The results for the rice field in the nights of July 27 and 29, 2000, are listed as cases 9 and 10 in Table 2. From the five cases of LST validation using vegetation sites, we can see that the error in MODIS LSTs in dense vegetation areas is compatible to and slightly larger than the cases of lake sites.

As shown by the MODIS snow cover product in early March 2001, the Bridgeport grassland was fully covered by snow on March 11, a clear-sky day. The two IR radiometers gave almost identical surface temperature at the time of night overpass of Terra. The MODIS LST, which is retrieved from MODIS L1B data in v3.0.0, well matches the in situ measured LST as shown in case 11 of Table 2. This is a good indication of the high quality of the MODIS TIR data in the B-side configuration.

6.3. Validation of the MODIS LST product using a silt playa in Railroad Valley, NV

In the last two sub-sections, the 1-km MODIS LSTs produced by the generalized split-window algorithm have been validated using lake sites and vegetation sites. We also conducted field campaigns over a silt playa in Railroad Valley, NV, in July 2001 in order to validate the MODIS LST products in semi-arid and arid regions where surface emissivities in bands 31 and 32 are more variable. The silt

Table 3

The difference between the 5-km LST retrieved by the day/night LST method and the LST aggregated from 1-km LSTs retrieved by the generalized split-window method is used to correct the effects associated with errors in the surface emissivities and atmospheric column water vapor used in the split-window method

Case no.	Site	Latitude, longitude	Date (month/day/year), time	View zenith azimuth (°)	Atmos. cwv (cm)	In situ T_s from radiometers (K) (no.)	Spatial variation ΔT_s (K)	MODIS T_s (ΔT_s) (K)	MODIS T_s (T_s (K), ΔT (K))	T_s in situ in situ T_s (K)	T_s in situ T_s (K)
1	Bridgeport snowcover	38.2199°N, 119.2683°W	3/11/01, 22:36 PST	40.48, -97.32	0.4	263.7 (2)	(0.2)	263.7 (0.2)	264.1 [0.43]	+0.4	+0.9
2	Railroad Valley, NV	38.4615°N, 115.6927°W	7/18/01, 10:35 PST	22.25, 99.48	1.25 (0.86)	321.6 (3)	0.8	318.54 (0.7)	321.5 [2.92]	-0.1	+0.2
3	Railroad Valley, NV	38.4617°N, 115.6926°W	7/19/01, 11:17 PST	47.36, -75.12	1.12	321.7 (3)	2.7	317.9 (1.8)	319.2 (0.5) [2.84]	+0.3	+0.1
4	Railroad Valley, NV	38.4617°N, 115.6926°W	7/19/01, 22:21 PST	43.78, -96.05	0.64	287.7 (3)	0.3	318.6 (1.3)	286.1 (0.4) [2.30]	+0.7	+0.6
5	Railroad Valley, NV	38.4616°N, 115.6928°W	7/20/01, 21:26 PST	44.40, 75.49	0.69	290.0 (4)	0.3	287.5 (0.2)	290.3 [2.83]	+0.3	+0.9
6	Railroad Valley, NV	38.4615°N, 115.6930°W	7/21/01, 11:05 PST	32.54, -77.26	0.68 (0.92)	320.6 (7)	0.4	287.5 (0.6)	317.7 (0.4) [3.20]	+0.3	+0.2
7	Railroad Valley, NV	38.4616°N, 115.6928°W	7/23/01, 21:57 PST	5.0, -98.04	1.01	291.1 (4)	0.5	317.2 (1.2)	288.8 (0.6) [2.19]	-0.1	-0.8

The difference between the corrected MODIS LST (T_s) and the in situ LST is shown in column 11. Direct validation of the 5-km LSTs is shown in the last column. Note that the T_s value in the first line of column 9 for each case is interpolated from the level-2 LST product and the values in the second line is the average and standard deviation of the T_s values at 5 × 5 grids in the MOD11A1 product. The ΔT value in the second line of column 10 for each case is the temperature difference given in Eq. (4).

playa has a size larger than 15×15 km at elevation of 1410 m above sea level. Fig. 5 shows the brightness temperature image calculated from band 45 radiance of MAS data collected in Railroad Valley on June 23, 1997. The brightness temperature varies a few degrees K in the central portion of the silt playa. As discussed in Section 5.2, the classification-based surface emissivities in bands 31 and 32 are overestimated in semi-arid and arid regions so that the 1-km MODIS LSTs retrieved by the split-window method would be underestimated. The 5-km MODIS LSTs retrieved by the day/night LST method should be better in semi-arid and arid regions because the surface emissivities are also retrieved simultaneously with the LST.

Before evaluating the 1- and 5-km MODIS LSTs, which are retrieved by two different methods, in semi-arid and arid regions, we compared them in a snowcover case in that we have relatively better knowledge of the surface emissivities. The Bridgeport grassland and its surroundings were fully covered by snow on March 11, 2001. As shown in the first case in Table 3, the difference between the 1- and 5-km MODIS LSTs is 0.3 K and the 1-km MODIS LST is larger than the in situ measured LST by 0.5 K. This case also indicates that the emissivities retrieved by the day/night method are underestimated by less than 0.01.

It will be ideal to find a large homogeneous site in semi-arid and arid areas so that we can accurately measure the surface temperature at the 5-km grid scale to validate the 5-km MODIS LST product. Unfortunately, we have not found such a site. So we take an alternative approach:

measure the surface temperature at the 1-km scale with multiple IR radiometers, aggregate the 1-km MODIS LSTs retrieved by the split-window method to the 5-km grids as used for the 5-km MODIS LSTs retrieved by the day/night method, calculate the difference between the aggregated 1-km LSTs and 5-km LSTs at four 5-km grids neighboring the in situ measurement points, interpolate the difference at the average position of the IR radiometers, and then add the interpolated difference onto the 1-km LST value to correct the effects associated with errors in the surface emissivities and atmospheric column water vapor used in the split-window method. We can express this approach in Eq. (4),

$$T_s^c(\text{lat}, \text{lon}) = T_{s,L2}(\text{lat}, \text{lon}) + T_{s,5 \text{ km}}(\text{lat}, \text{lon}) - T_{s,1 \text{ km} \rightarrow 5 \text{ km}}(\text{lat}, \text{lon}), \quad (4)$$

where $T_{s,L2}(\text{lat}, \text{lon})$ is the LST at geolocation (lat,lon) interpolated from the LSTs at nearest pixels in the MOD11_L2 product, $T_{s,5 \text{ km}}(\text{lat}, \text{lon})$ is the LST interpolated from the 5-km LSTs at nearest grids in the MOD11B1 product, $T_{s,1 \text{ km} \rightarrow 5 \text{ km}}(\text{lat}, \text{lon})$ is the LST interpolated from SDS LST_Day_5km_Aggregated_from_1km or LST_Night_5km_Aggregated_5 from_1km at nearest 5-km grids in the MOD11B1 product. Note that we make the 2D interpolation with the latitude and longitude values of the averaged location of the in situ measurement points, and the latitude and longitude values of the nearest pixels or grids.

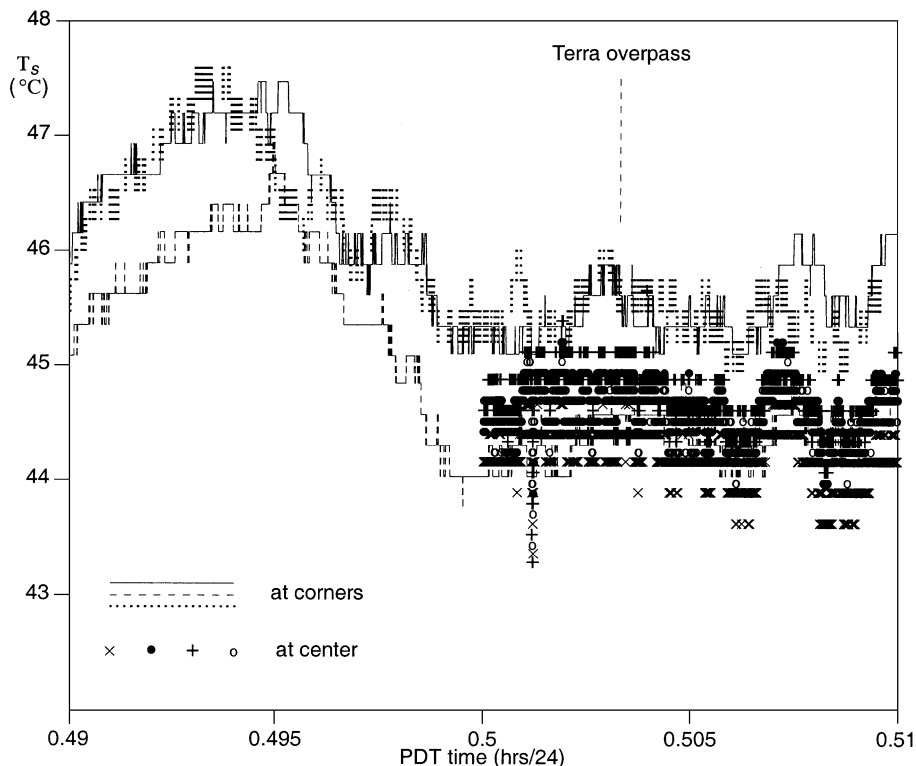


Fig. 6. Surface temperatures measured by seven radiometers in Railroad Valley, NV, on July 21, 2001.

This is more appropriate than an alternative interpolation with the line and sample numbers (or row and column numbers) and their fractions of the averaged location of the in situ measurement points. Different interpolation schemes will give slightly different results.

Cases 2–7 in Table 3 are the six comparisons made for the MODIS LST products with the in situ measurement data that we collected over the silt playa in Railroad Valley, NV. Following the same procedures used in Wan et al. (2002), the emissivity effect on the LSTs measured by the IR radiometers is calculated based on the spectral emissivity averaged from our measurements of silt playa samples collected from the site, typical atmospheric temperature and water vapor profiles measured at the site, and the spectral response function of the IR radiometer. It is 2.3 K with an estimated uncertainty slightly less than 1 K due to the spatial variation in the surface emissivities. Fig. 6 shows the playa surface temperatures measured by seven radiometers in Railroad Valley, NV, on July 21, 2001. The solid, dashed, and dotted lines represent the surface temperatures measured by three IR radiometers located at corners of a rectangle of 100×100 m. The four symbols represent the surface temperatures measured by four IR radiometers

located at the center of the rectangle. In order to measure the viewing angle effect, these four IR radiometers were placed in a box in a such way that they viewed the same portion on the surface at a zenith angle of 15° from nadir and in the four azimuth directions of E, S, W, and N. In this case, there were significant temporal variations in the measured LSTs before noon, the spatial variations were about 1 K, and the viewing angle effect was less than 0.3 K. Fortunately, the temporal variation was smaller around the time of Terra overpass. In Table 3, columns 1–8 are similar to those in Table 2, column 9 is for the 1-km MODIS LST, and column 10 is for T_s^c (the 1-km MODIS LST after the correction with the 5-km MODIS LST), and column 11 is for the difference between T_s^c and the in situ measured LSTs. Note that the T_s value in the first line of column 9 for each cases is interpolated from the level-2 LST product and the values in the second line is the average and standard deviation of the T_s values at 5×5 grids in the MOD11A1 product. The ΔT value in the second line of column 10 for each case is the temperature difference $T_{s,5 \text{ km}}(\text{lat}, \text{lon}) - T_{s,1 \text{ km} \rightarrow 5 \text{ km}}(\text{lat}, \text{lon})$ in Eq. (4). If we compare the values in the first line of columns 7 and 9 for cases 2–7, we find that the 1-km MODIS LSTs retrieved by the split-window method

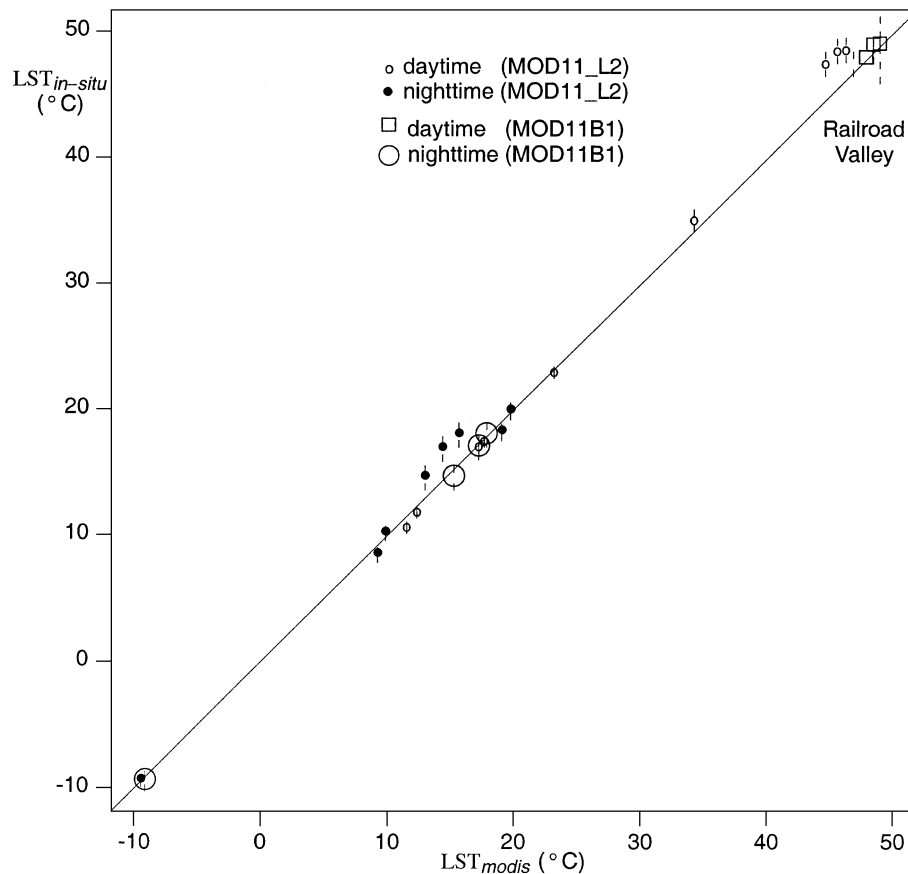


Fig. 7. Comparisons between the MODIS LSTs and the LSTs from in situ measurements. The $LST_{in\ situ}$ ($^{\circ}C$) values are calculated from the values in column 7 of Tables 2 and 3. The LST_{MODIS} ($^{\circ}C$) values are calculated from column 10 in Table 2 and column 9 in Table 3 for the direct validation of 1-km LSTs in the MOD11_L2 product, and from column 10 in Table 3 for the indirect validation of 5-km LSTs in the MOD11B1 product. The results of direct comparisons between the 5-km LSTs and the in situ LSTs are shown in the last column of Table 3.

are underestimated by -1.6 to -3.1 K at different viewing angles under different atmospheric conditions. After the correction with the 5-km MODIS LSTs retrieved by the day/night method, the differences reduce to the range from -0.1 to 0.7 K in the six cases. We consider the values in column 11 of Table 3 as indirect validations of the 5-km MODIS LST product.

We also made direct comparisons of the 5-km LST values to the in situ LST values for the seven cases. The difference values are within ± 1 K as shown in the last column of Table 3. However, we do not have a high confidence in this direct validation of the 5-km LST because of the uncertainty in LST spatial variations within the 5-km grid.

6.4. Summary of the validation results

All the direct validation results in Table 2 and indirect validation results in Table 3 column 11 are presented in Fig. 7 in order to show the range of LSTs in the validations. The height of the vertical dashed line at each data point represents the uncertainty in the in situ LST value. The error associated with the uncertainty in surface emissivities is 0.2, 0.5, and 0.9 K for lake, grassland/snowcover/rice field, and silt playa sites, respectively. In summary, the MODIS LST products were validated in 18 cases in the LST range from 263 to 322 K and the atmospheric column water vapor range from 0.4 to 3.0 cm.

7. Conclusion

A double-screen scheme based on the difference between the 5-km LST retrieved by the day/night LST algorithm and the aggregated 1-km LST retrieved by the generalized split-window algorithm, and the difference between daytime and nighttime LSTs, is proposed to remove the LSTs contaminated with cloud effects. The accuracy of daily MODIS LST product at 1-km resolution, which was produced by the generalized split-window algorithm, was validated in 11 clear-sky cases with in situ measurement data collected in field campaigns in 2000 and 2001. The MODIS LST accuracy is better than 1 K in the range from 263 to 300 K over Lake Titicaca in Bolivia, Mono Lake, Bridgeport grassland, and a rice field in Chico, CA, and Walker Lake, NV, in the atmospheric column water vapor range from 0.4 to 3.0 cm. In six cases over a silt playa in Railroad Valley, NV, the 1-km MODIS LSTs are a few Kelvin degrees lower than the in situ measured LSTs because the surface emissivities inferred from land cover types in the split-window LST method are often overestimated in semi-arid and arid regions. After a correction with the difference between the 5-km LST retrieved by the day/night LST method and the LST aggregated from 1-km LSTs retrieved by the split-window method, the MODIS LSTs agree with in situ measured LSTs well within ± 1 K in the range from 263

to 322 K for the six cases in Railroad Valley and one case of snowcover in Bridgeport, CA. In these seven cases, the 5-km LST values retrieved by the day/night LST method also agree with the in situ measured LSTs within ± 1 K with a larger uncertainty due to the LST spatial variation within the 5-km grid. It is recommended that the 1-km LST product retrieved by the generalized split-window LST method be used for lakes, snow/ice, and dense vegetated areas, and the 5-km LST product retrieved by the day/night LST method be used in bare and sparse vegetated areas.

Acknowledgements

This work was supported by EOS Program contract NAS5-31370 of the National Aeronautics and Space Administration. The field campaign activities conducted in Bridgeport, CA, were partly supported by NASA grant NAG13-99023, in which Dr. Kenneth W. Tate, University of California at Davis is PI, and Dr. Zhengming Wan is co-PI. The authors would like to thank Dr. Robert Jellison, University of California/Sierra Nevada Aquatic Research Lab., Dr. Richard E. Plant, University of California at Davis, Mr. Stan Hunewill and Jeff Hunewill, Hunewill Guest Ranch, Bridgeport, CA, for their supports in the LST validation activities, the staffs at Airborne Sensor Facility, NASA Ames Research Center, and at the ER-2 Operations Office, NASA Dryden Flight Research Center, for providing the MAS data. The MODIS data were generated by the Goddard DAAC under supports of MODIS MCST and SDDT. The MODIS LST product was generated by the MODAPS under supports of MODIS SDDT, its routine quality assessment was performed by the LDOPE, and the LST product was distributed by the EDC DAAC. The authors would like to thank John C. Price and other two anonymous reviewers for their valuable comments and suggestions, which helped to improve the paper.

References

- Becker, F. (1987). The impact of spectral emissivity on the measurement of land surface temperature from a satellite. *International Journal of Remote Sensing*, 8(10), 1509–1522.
- Becker, F., & Li, Z.-L. (1990). Toward a local split window method over land surface. *International Journal of Remote Sensing*, 11(3), 369–393.
- Berk, A., Anderson, G. P., Bernstein, L. S., Acharya, P. K., Dothe, H., Matthew, M. W., Adler-Golden, S. M., Chetwynd Jr., J. H., Richtmeier, S. C., Pukall, B., Allred, C. L., Jeong, L. S., & Hoke, M. L. (1999). MODTRAN4 radiative transfer modeling for atmospheric correction. *Optical Spectroscopic Techniques and Instrumentation for Atmospheric and Space Research III. Proceedings of SPIE*, vol. 3756 (pp. 348–353).
- Brown, O. B., Evans, R. H., & Cornillon, P. (1991). Satellite-derived global sea surface temperature fields: 1982–1989. *Global and Planetary Change*, 90, 179–181.
- Bruegge, C. J., Conel, J. E., Green, R. O., Margolis, J. S., Holm, R. G., & Toon, G. (1992). Water vapor column abundance retrievals during FIFE. *Journal of Geophysical Research*, 97(D17), 18759–18768.
- Brutsaert, W., Hsu, A. Y., & Schmugge, T. J. (1993). Parameterization of

- surface heat fluxes above forest with satellite thermal sensing and boundary-layer soundings. *Journal of Applied Meteorology*, 32(5), 909–917.
- Caselles, V., & Sobrino, J. A. (1989). Determination of frosts in orange groves from NOAA-9 AVHRR data. *Remote Sensing of Environment*, 29(2), 135–146.
- Chedin, A., Scott, M. A., Wahiche, C., & Moulinier, P. (1985). The improved initialization inversion method: a high resolution physical method for temperature retrievals from the Trios-N series. *Journal of Climate and Applied Meteorology*, 24, 124–143.
- Diak, G. R., & Whipple, M. S. (1993). Improvements to models and methods for evaluating the land-surface energy balance and effective roughness using radiosonde reports and satellite-measured skin temperature data. *Agricultural and Forest Meteorology*, 63 (3–4), 189–218.
- Ehrlich, D., & Lambin, E. F. (1996). The surface temperature–vegetation index space for land cover and land-cover change analysis. *International Journal of Remote Sensing*, 17(3), 463–487.
- Esaías, W. E., Abbott, M. R., Barton, I., Brown, O. W., Campbell, J. W., Carder, K. L., Clark, D. K., Evans, R. L., Hoge, F. E., Gordon, H. R., Balch, W. P., Letelier, R., & Minnett, P. J. (1998). An overview of MODIS capabilities for ocean science observations. *IEEE Transactions on Geoscience and Remote Sensing*, 36(4), 1250–1265.
- Feldhake, C. M., Glenn, D. M., & Peterson, D. L. (1996). Pasture soil surface temperature response to drought. *Agronomy Journal*, 88 (4), 652–656.
- French, A. N., Schmugge, T. J., & Kustas, W. P. (2000a). Discrimination of senescent vegetation using thermal emissivity contrast. *Remote Sensing of Environment*, 74(2), 249–254.
- French, A. N., Schmugge, T. J., & Kustas, W. P. (2000b). Estimating surface fluxes over the SGP site with remotely sensed data. *Physics and Chemistry of the Earth. Part B: Hydrology Oceans and Atmosphere*, 25(2), 167–172.
- Fuchs, M., & Tanner, C. B. (1966). Infrared thermometry of vegetation. *Agronomy Journal*, 58, 597–601.
- Gao, B. C., & Kaufman, Y. J. (1995). Selection of the 1.375 μm MODIS channel for remote sensing of cirrus cloud and stratospheric aerosols from space. *Journal of Atmospheric Sciences*, 52(23), 4231–4237.
- Gillespie, A. (1985). Lithologic mapping of silicate rocks using TIMS. *TIMS Data Users' Workshop. JPL Publication, vol 86-38* (pp. 29–44). Pasadena, CA: Jet Propul. Lab.
- Gillespie, A. R., Rokugawa, S., Matsunaga, T., Cothorn, J. S., Hook, S., & Kahle, A. B. (1998). A temperature and emissivity separation algorithm for Advanced Spaceborne Thermal Emission and Reflection Radiometer (ASTER) images. *IEEE Transactions on Geoscience and Remote Sensing*, 36, 1113–1126.
- Jackson, R. D., Reginato, R. J., & Idso, S. B. (1977). Wheat canopy temperature: a practical tool for evaluating water requirements. *Water Resources Research*, 13, 651–656.
- Jin, M. J., & Dickinson, R. E. (1999). Interpolation of surface radiative temperature measured from polar orbiting satellites to a diurnal cycle—1. Without clouds. *Journal of Geophysical Research*, 104(ND2), 2105–2116.
- Justice, C. O., Vermote, E., Townshend, J. R. G., Defries, R., Roy, D. O., Hall, D. K., Salomonson, V. V., Privette, J. L., Riggs, G., Strahler, A., Lucht, W., Myneni, R. B., Knyazikhin, K., Running, S. W., Nemani, P. R., Wan, Z., Huete, A. R., van Leeuwen, W., Wolfe, R. E., Giglio, L., Muller, J.-P., Knyazikhin, Y., & Barnsley, M. J. (1998). The Moderate Resolution Imaging Spectroradiometer (MODIS): land remote sensing for global change research. *IEEE Transactions on Geoscience and Remote Sensing*, 36, 1228–1249.
- Kahle, A. B., Madura, D. P., & Soha, J. M. (1980). Middle infrared multi-spectral aircraft scanner data: analysis for geological applications. *Applied Optics*, 19, 2279–2290.
- Kaufman, Y. J., Justice, C. O., Flynn, L. P., Kendall, L. D., Prins, E. M., Giglio, L., Ward, D. E., Menzel, W. P., & Setzer, A. W. (1998). Potential global fire monitoring from EOS-MODIS. *Journal of Geophysical Research*, 103(D24), 32215–32238.
- Kealy, P. S., & Gabell, A. R. (1990). Estimation of emissivity and temperature using alpha coefficients. *Proc. 2nd TIMS Workshop. JPL Publication, vol 90–55*, (pp. 11–15). Pasadena, CA: Jet Propul. Lab.
- Kerr, Y. H., Lagouarde, J. P., & Imbernon, J. (1992). Accurate land surface temperature retrieval from AVHRR data with use of an improved split window algorithm. *Remote Sensing of Environment*, 41(2–3), 197–209.
- King, M. D., Kaufman, Y. J., Menzel, W. P., & Tanré, D. (1992). Remote sensing of cloud, aerosol, and water vapor properties from the Moderate Resolution Imaging Spectrometer (MODIS). *IEEE Transactions on Geoscience and Remote Sensing*, 30(1), 2–27.
- Lambin, E. F., & Ehrlich, D. (1997). Land-cover changes in sub-Saharan Africa (1982–1991): application of a change index based on remotely sensed surface temperature and vegetation indices at a continental scale. *Remote Sensing of Environment*, 61(2), 181–200.
- Li, Z.-L., & Becker, F. (1993). Feasibility of land surface temperature and emissivity determination from AVHRR data. *Remote Sensing of Environment*, 43, 67–85.
- Li, Z.-L., Becker, F., Stoll, M. P., & Wan, Z. (1999). Evaluation of six methods for extracting relative emissivity spectra from thermal infrared images. *Remote Sensing of Environment*, 69, 197–214.
- Ma, X., Wan, Z., Moeller, C. C., Menzel, W. P., Gumley, L. E., & Zhang, Y. (2000). Retrieval of geophysical parameters from Moderate Resolution Imaging Spectroradiometer thermal infrared data: evaluation of a two-step physical algorithm. *Applied Optics*, 39(20), 3537–3550.
- Ma, X.-L., Wan, Z., Moeller, C. C., Menzel, W. P., & Gumley, L. E. (2002). Simultaneous retrieval of atmospheric profiles and land-surface temperature, and surface emissivity from Moderate Resolution Imaging Spectroradiometer thermal infrared data: extension of a two-step physical algorithm. *Applied Optics*, 41(20), 909–924.
- Mannstein, H. (1987). Surface energy budget, surface temperature and thermal inertia. In R. A. Vaughan, & D. Reidel (Eds.), *Remote Sensing Applications in Meteorology and Climatology. NATO Advanced Study Institutes Series. Series C, Mathematical and Physical Sciences, vol 201* (pp. 391–410). Dordrecht, The Netherlands: A. Reidel Publishing.
- McVicar, T. R., & Jupp, D. L. B. (1998). The current and potential operational uses of remote sensing to aid decisions on drought exceptional circumstances in Australia: a review. *Agricultural Systems*, 57(3), 399–468.
- Muchoney, D. M., Borak, J. S., Chi, H., Friedl, M., Hodges, J., Morrow, N., & Strahler, A. (1999). Application of the MODIS global supervised classification model to vegetation and land cover mapping of Central America. *International Journal of Remote Sensing*, 21(6/7), 1115–1138.
- Nerry, F., Petitcolin, F., & Stoll, M. P. (1998). Bidirectional reflectivity in AVHRR channel 3: application to a region in Northern Africa. *Remote Sensing of Environment*, 66, 298–316.
- Ottlé, C., & Stoll, M. (1993). Effect of atmospheric absorption and surface emissivity on the determination of land temperature from infrared satellite data. *International Journal of Remote Sensing*, 14(10), 2025–2037.
- Ottlé, C., & Vidal-Madjar, D. (1992). Estimation of land surface temperature with NOAA9 data. *Remote Sensing of Environment*, 40(1), 27–41.
- Padilla, H. G., Leyva, A. C., & Mosino, P. A. (1993). An analysis of daily humidity patterns at a mountainous and urban site in a tropical high-altitude region. *Journal Applied Meteorology*, 32, 1638–1646.
- Plokhenko, Y., & Menzel, W. P. (2000). The effects of surface reflection on estimating the vertical temperature–humidity distribution from spectral infrared measurements. *Journal of Applied Meteorology*, 39, 3–14.
- Prata, A. J. (1994). Land surface temperatures derived from the advanced very high resolution radiometer and the along-track scanning radiometer: 2. Experimental results and validation of AVHRR algorithms. *Journal of Geophysical Research*, 99(D6), 13025–13058.
- Price, J. C. (1982). On the use of satellite data to infer surface fluxes at meteorological scales. *Journal of Applied Meteorology*, 21, 1111–1122.
- Price, J. C. (1983). Estimating surface temperature from satellite thermal infrared data—a simple formulation for the atmospheric effect. *Remote Sensing of Environment*, 13, 353–361.
- Price, J. C. (1984). Land surface temperature measurements from the split

- window channels of the NOAA-7 AVHRR. *Journal of Geophysical Research*, 79, 5039–5044.
- Realmuto, V. J. (1990). Separating the effects of temperature and emissivity: emissivity spectrum normalization. *Proc. 2nd TIMS Workshop. JPL Publication, vol 90-55* (pp. 23–27). Pasadena, CA: Jet Propul. Lab.
- Salomonson, V., Barnes, W., Maymon, P., Montgomery, H., & Ostrow, H. (1989). MODIS: advanced facility instrument for studies of the Earth as a system. *IEEE Transactions on Geoscience and Remote Sensing*, 27(2), 145–153.
- Sellers, P. J., Hall, F. G., Asrar, G., Strelbel, D. E., & Murphy, R. E. (1988). The first ISLSCP Field Experiment (FIFE). *Bulletin of the American Meteorological Society*, 69(1), 22–27.
- Smith, T. M., & Reynolds, R. W. (1998). A high-resolution global sea surface temperature climatology for the 1961–90 base period. *Journal of Climate*, 11, 3320–3323.
- Smith, W. L., Woolf, H. M., & Schriener, A. J. (1985). Simultaneous retrieval of surface and atmospheric parameters: a physical and analytically direct approach. In A. Deepak, H. E. Fleming, & M. T. Chahine (Eds.), *Advances in Remote Sensing Retrieval Methods* (pp. 221–232). Hampton, VA, USA: A. Deepak Publishing.
- Snyder, W., & Wan, Z. (1998). BRDF models to predict spectral reflectance and emissivity in the thermal infrared. *IEEE Transactions on Geoscience and Remote Sensing*, 36(1), 214–225.
- Snyder, W., Wan, Z., Zhang, Y., & Feng, Y.-Z. (1997a). Requirements for satellite land surface temperature validation using a silt playa. *Remote Sensing of Environment*, 61(2), 279–289.
- Snyder, W., Wan, Z., Zhang, Y., & Feng, Y.-Z. (1997b). Thermal infrared (3–14 μm) bidirectional reflectance measurements of sands and soils. *Remote Sensing of Environment*, 60, 101–109.
- Snyder, W. C., Wan, Z., Zhang, Y., & Feng, Y.-Z. (1998). Classification-based emissivity for land surface temperature measurement from space. *International Journal of Remote Sensing*, 19(14), 2753–2774.
- Sobrino, J. A., Coll, C., & Caselles, V. (1991). Atmospheric corrections for land surface temperature using AVHRR channel 4 and 5. *Remote Sensing of Environment*, 38(1), 19–34.
- Susskind, J., Rosenfield, J., Reuter, D., & Chahine, M. T. (1984). Remote sensing of weather and climate parameters from HIRS2/MSU on TIROS-N. *Journal of Geophysical Research*, 89(D3), 4677–4697.
- Townshend, J. R. G., Justice, C. O., Skole, D., Malingreau, J.-P., Cihlar, J., Teillet, P., & Ruthenberg, S. (1994). The 1 km resolution global data set: needs of the international geosphere biosphere programme. *International Journal of Remote Sensing*, 15, 3417–3441.
- Vidal, A. (1991). Atmospheric and emissivity correction of land surface temperature measured from satellite using ground measurements or satellite data. *International Journal of Remote Sensing*, 12(12), 2449–2460.
- Wan, Z. (2002). Estimate of noise and systematic error in early thermal infrared data of the Moderate Resolution Imaging Spectroradiometer (MODIS). *Remote Sensing of Environment*, 80(1), 47–54.
- Wan, Z., & Dozier, J. (1989). Land-surface temperature measurement from space: physical principles and inverse modeling. *IEEE Transactions on Geoscience and Remote Sensing*, 27(3), 268–278.
- Wan, Z., & Dozier, J. (1996). A generalized split-window algorithm for retrieving land-surface temperature from space. *IEEE Transactions on Geoscience and Remote Sensing*, 34(4), 892–905.
- Wan, Z., & Li, Z.-L. (1997). A physics-based algorithm for retrieving land-surface emissivity and temperature from EOS/MODIS data. *IEEE Transactions on Geoscience and Remote Sensing*, 35(4), 980–996.
- Wan, Z., Zhang, Y., Li, Z.-L., Wang, R., Salomonson, V. V., Yves, A., & Bosseno, R. (2002). Preliminary estimate of calibration of the Moderate Resolution Imaging Spectroradiometer (MODIS) thermal infrared data using Lake Titicaca. *Remote Sensing of Environment*, 80(3), 497–515.
- Watson, K. (1992). Spectral ratio method for measuring emissivity. *Remote Sensing of Environment*, 42, 113–116.